ARTICLE IN PRESS

Hydrophobin-stabilized dispersions of PVDF nanoparticles in water

Claudia Pigliacelli [a], Alessandro D'Elicio [a], Roberto Milani [b], Giancarlo Terraneo [a], Giuseppe Resnati [a,**], Francesca Baldelli Bombelli [a,**], Pierangelo Metrangolo [a,b,*]

[a] Laboratory of Nanostructured Fluorinated Materials (NFMLab), Fondazione Centro Europeo Nanomedicina c/o Department of Chemistry, Materials, and Chemical Engineering "Giulio Natta", Politecnico di Milano, Via L. Mancinelli 7, 20131 Milan, Italy
[b] VTT-Technical Research Centre of Finland, FI-02044 VTT, Espoo, Finland

A B S T R A C T

In this study, aqueous dispersions of partially crystalline PVDF nanoparticles (NPs) were obtained employing hydrophobin (HFB), an amphiphilic film-forming protein able to film hydrophobic surfaces. Dynamic Light Scattering (DLS) and Transmission Electron Microscopy (TEM) analysis of PVDF-HFBII aqueous dispersions confirmed the HPBII ability to film PVDF hydrophobic NPs. Freeze-dried PVDF-HFBII bio-nanocomposites were shown to be effectively re-dispersible in water. An aqueous dispersion of PVDF NPs may have an impact on the applications of this polymer in the perspective of the development of environmentally friendly coating methods.

© 2015 The Authors. Published by Elsevier B.V. This is an open access article under the CC BY-NC-ND license (http://creativecommons.org/licenses/by-nc-nd/4.0/).
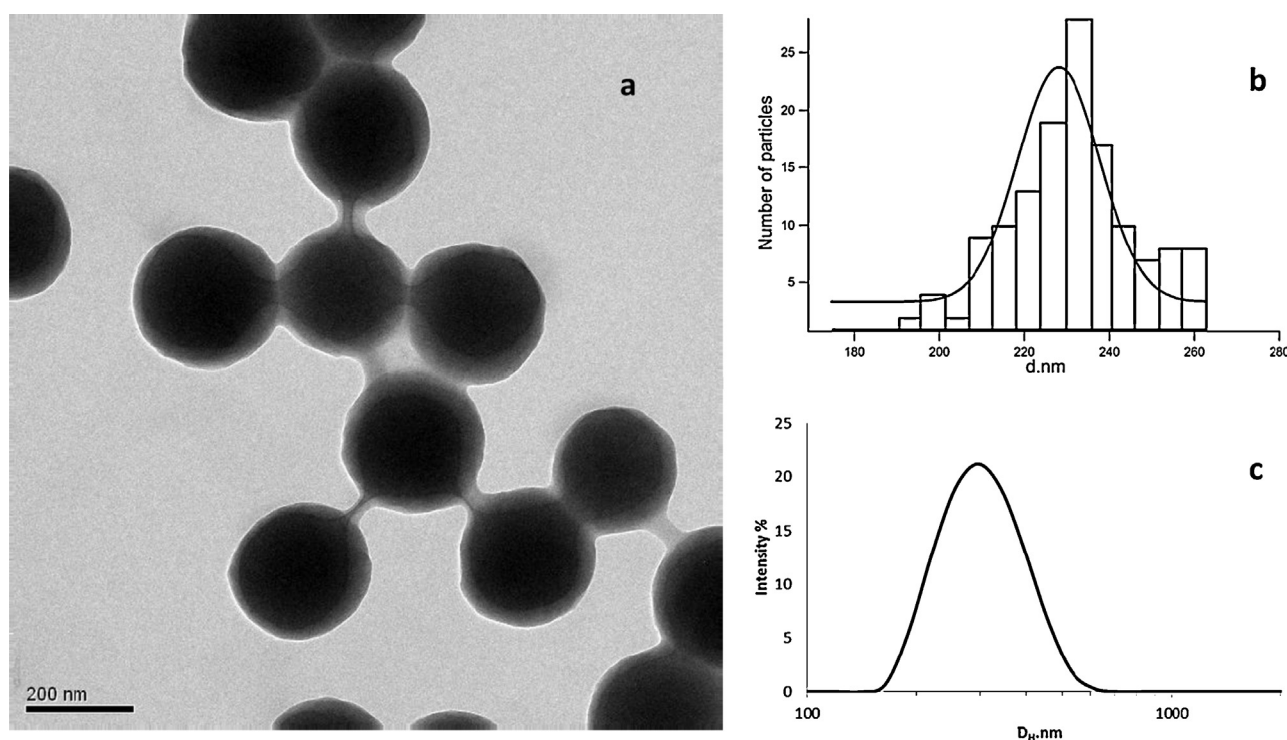
1. Introduction

Since its discovery and commercial introduction in the 1960s, poly(vinylidene fluoride) (PVDF) has gained a growing attention in both industrial and scientific fields, due to its unique physical and chemical properties. Piezoelectric, pyroelectrical, and ferroelectric behaviours of PVDF have widely been studied and characterized [1–3], and promoted the use of PVDF in electrical and electronic devices [4,5]. Thanks to its fluorination degree, PVDF is characterized by high thermal stability, mechanical, and chemical resistance, making it also an excellent membrane material [6]. Recently the synthesis of silica nanoparticles functionalized with PVDF chains was reported in literature highlighting possible innovative applications of PVDF in the production of nanocomposites [7–10]. Additionally, PVDF is widely employed in paints and coatings,

thanks to its low surface energy, which renders PVDF an excellent polymer for the surface functionalization of materials, in order to improve metallic substrates resistance to weather, corrosion, and chemicals [11]. These excellent properties and the wide range of applications contrast with some limitations in PVDF use resulting from its poor water-solubility. In fact, due to its hydrophobic nature, the use of organic solvents and/or melting processing of the polymer are necessary for its manufacture and uses, increasing the costs and possible toxicity implications related to solvent handling. A water-based PVDF formulation might further promote PVDF use. In this regard, Kynar Aquatec®, a water-based PVDF formulation, represents a coating emulsion that has been shown to offer the same material protection and durability of organic solvent-based PVDF coatings [12]. Therefore, the development of new PVDF water-based formulations might further promote the application of such versatile polymer in different fields. One of the most promising and sustainable approaches for improving the solubility of poorly water-soluble materials is represented by the use of biosurfactants. In this regard, hydrophobins (HFBs) are a class of small, highly surface-active proteins (7–10 kDa) produced by filamentous fungi [13]. HFBs play an important role in different stages of the fungal cell development and in its protection. In particular, thanks to their surface activity, they coat and protect different fungal structures and allow fungal attachment to surfaces. HFBs' structure is characterized

Fig. 1. (a) TEM image of PVDF pristine NPs, bar = 200 nm. (b) Size distribution histogram obtained by size analysis of several TEM images of particles (about 130 NPs) to obtain meaningful statistical results for the particle size. (c) DLS intensity-weighted size distribution obtained by CONTIN of 1 mg/mL PVDF NPs dispersion in MEK.

by a conserved pattern of eight cysteine residues that form four disulfide bridges [14]. HFBs are amphiphilic and the self-assembling and filming abilities of these proteins are associated with the hydrophobic patch composed of the aliphatic chains of a part of their amino acid sequences [15]. In fact, HFBs are able to form amphiphilic films at both air/water and hydrophobic/hydrophilic interfaces [16]. Two classes of HFBs have been reported in the literature [13]. Class I HFBs form aggregates that show limited solubility in aqueous solutions, while class II HFBs self-assemble in more water-soluble aggregates [17]. HFBs' coating ability can potentially be exploited in different applications and their possible use in materials, nutraceutical, pharmaceutical, and nanomedical fields have recently been regarded [15,17–19]. HFB was shown to significantly impact the adsorption of proteins on the surface of nanoparticles, once they are exposed to biological fluids, reducing the formation of the protein corona [19], which has been proved to dramatically influence nanoparticles behaviour in the biological environment [20]. Moreover, Milani et al. reported the HFB's ability to stabilize fluorous droplets in aqueous environment, proving its potential as *fluorine-free* fluorosurfactant [21].
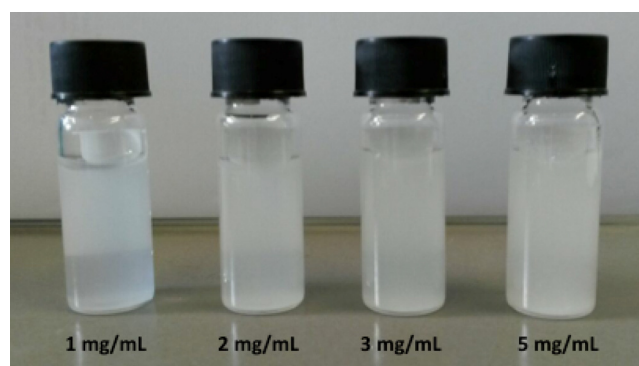
In this study, we focused on the possible dispersion of PVDF NPs in water through surface coating with class II hydrophobins HFBI and HFBII. HFBs' biocompatibility, their ability to form robust films, and reverse surface wettability make them promising candidates for this scope. Class I HFBs have been proven to film hydrophobic surfaces *via* the formation of rodlet structures [22,23]. As far as class II HFBs are concerned, their remarkable ability to increase the wettability of hydrophobic particles has been shown by adsorption studies on Teflon®, Kevlar®, and other substrates[15]. In our study, four increasing concentrations of PVDF NPs were successfully dispersed in HFBII aqueous solutions. The polymeric NPs were filmed by HFBII and the resulting structures were investigated by TEM and DLS analyses and compared to pristine PVDF NPs dispersed in Methyl Ethyl Ketone (MEK). HFBI ability to transfer PVDF NPs into water dispersions was also evaluated. Obtained dispersions were subsequently freeze-dried and characterized by

attenuated total reflectance infrared spectroscopy (ATR-FTIR), differential scanning calorimetry (DSC), and powder X-ray diffraction (PXRD) analyses. Solid state analysis was performed for evaluating the possible impact of the dispersion protocol on the PVDF crystallinity content and polymorphism, and for investigating the protein secondary structure when adsorbed on the PVDF surface. Particular attention was paid to the characterization of the freeze-dried PVDF-HFBII bio-nanocomposites in the perspective to re-disperse them in water. Indeed, this would allow the preparation of water-soluble PVDF bio-nanocomposites, which to date have not been reported, yet.
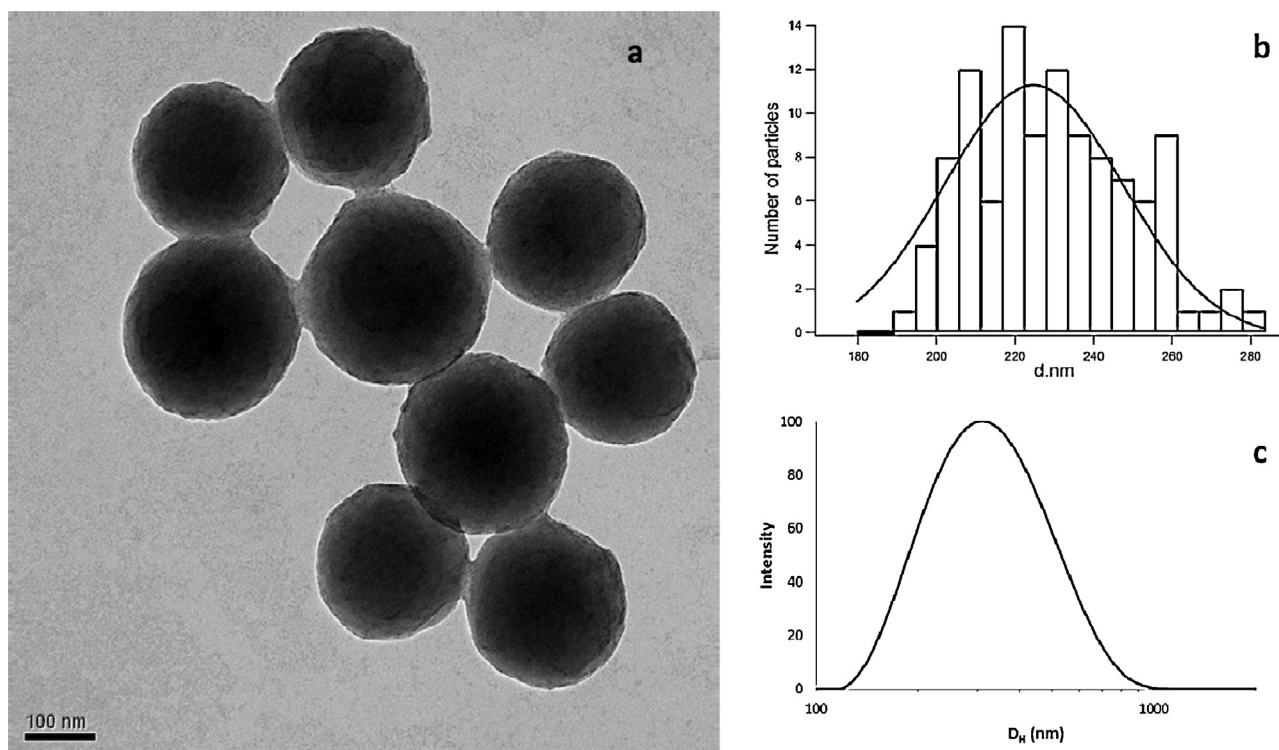
2. Results and discussion

2.1. PVDF dispersions in organic and aqueous environments

PVDF has been shown to be dispersible in Methyl Ethyl Ketone (MEK) [24]. PVDF dispersions in MEK (1 mg/mL) were prepared by

Fig. 2. PVDF-HFBII aqueous dispersions at the concentration of 1, 2, 3, and 5 mg/mL after 24 h at room temperature from preparation.
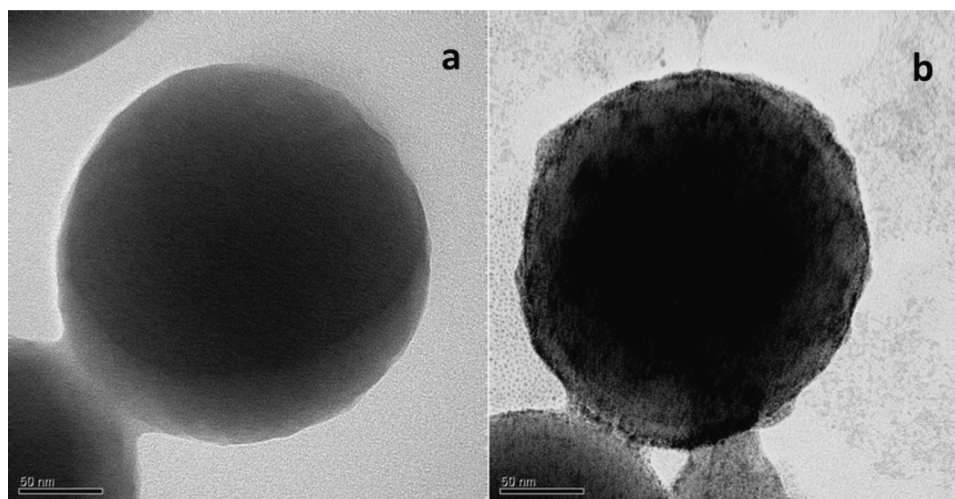
Fig. 3. (a) TEM image of HFBII coated PVDF NPs, bar = 100 nm. (b) Size distribution histogram obtained by size analysis of several TEM images of particles (about 110 NPs) to obtain meaningful statistical results for the particle size. (c) DLS intensity-weighed size distribution obtained by CONTIN of 1 mg/mL PVDF NPs dispersed in a solution of HFBII (0.1 mg/mL) in water.

simple magnetic stirring and analyzed after 24 h. As shown by TEM images (see Fig. 1a), PVDF dispersions in MEK afforded mono-dispersed round-shaped NPs of an average size of 228 ± 31 nm (Fig. 1b). DLS analysis yielded an average hydrodynamic diameter of 256 ± 2 nm (see the hydrodynamic size distribution in Fig. 1c).

PVDF dispersions in aqueous HFBII solutions were prepared by ultrasonication. The provision of highly localized energy was essential for the polymer dispersion in the protein solution. Indeed, the use of other approaches such as magnetic stirring, vortex, and ultrasounds bath failed in dispersing PVDF in HFBII solutions. PVDF concentrations from 1 to 5 mg/mL were successfully dispersed in 0.1 mg/mL HFBII aqueous solutions, forming opalescent dispersions
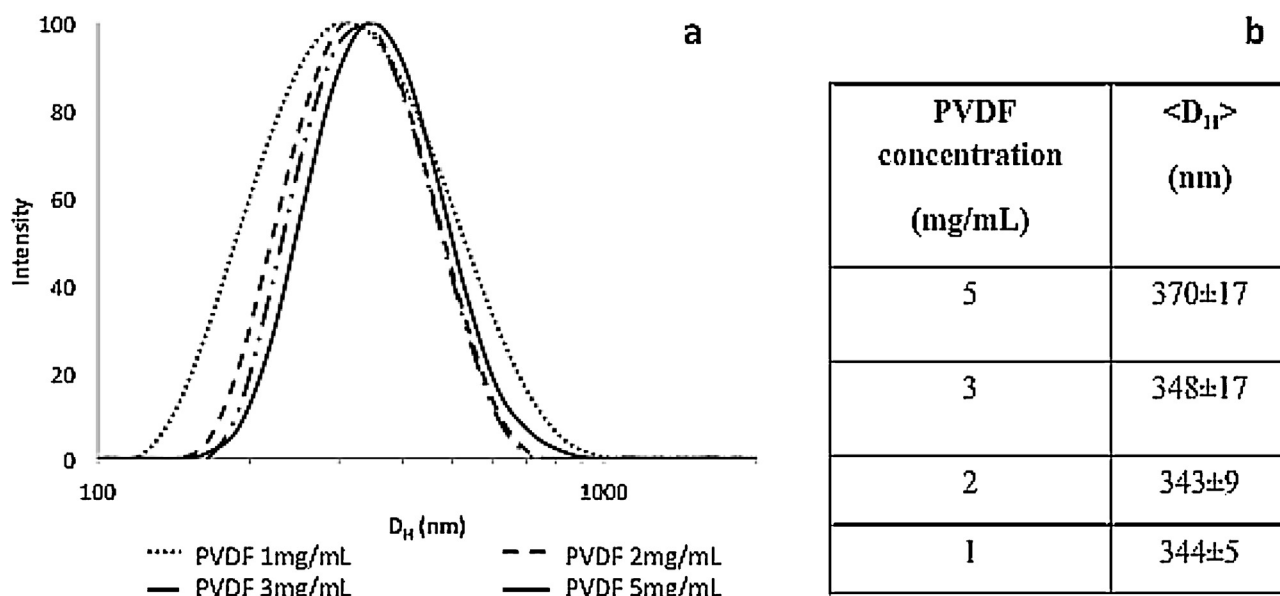
that did not display significant sedimentation over 24 h, as shown in Fig. 2. PVDF dispersions at polymer concentrations higher than 5 mg/mL presented, instead, extensive sedimentation within one hour from preparation (see Fig. S1 in ESI).

The formation of a monolayer of HFBII has been reported to correspond to a surface coverage in the 200–250 ng/cm^2 range [25], and previous work showed a filming ability of HFBII towards TE5069 Teflon® particles of about 125 ng of protein per cm^2 of particles [26]. The surface area of our PVDF nanoparticles can be roughly approximated as 150 cm^2/mg, as calculated for a population of uniformly sized nanoparticles with a radius of 114 nm and a density of 1.75 g/cm^3. According to this approximation, HFBII has a

Fig. 4. (a) TEM analysis of pristine PVDF NPs (dried from MEK); (b) TEM analysis of HFBII coated PVDF NPs (dried from water and stained with uranyl acetate). Bar = 50 nm. TEM image (b) shows the presence of HFBII aggregates in solution (grey islets on the carbon grid), for which the formation has already been described in the literature [28].
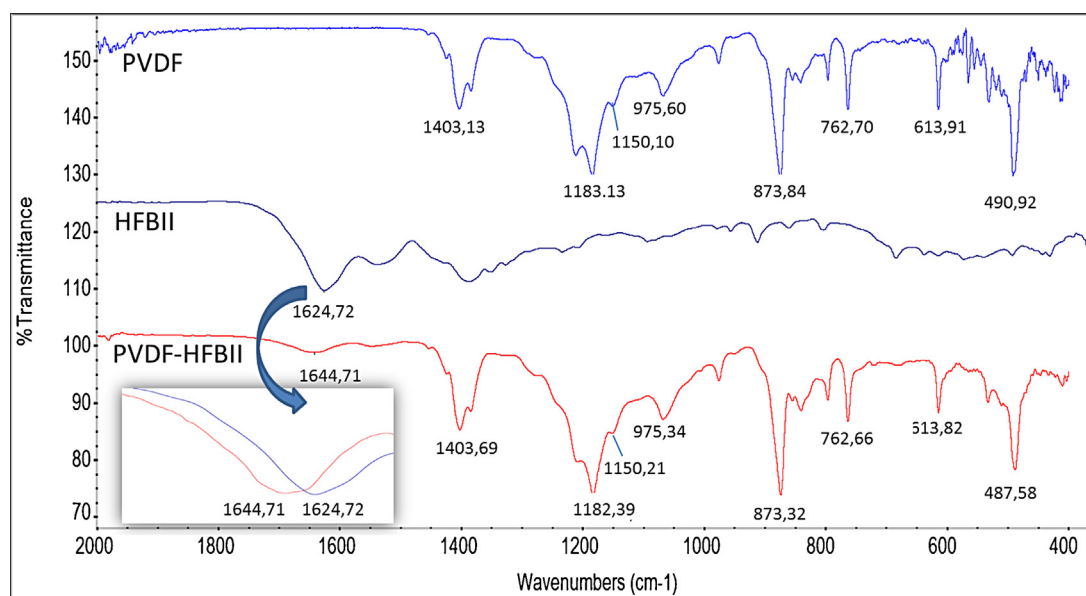
PVDF concentration (mg/mL)	$\langle D_H \rangle$ (nm)
5	370±17
3	348±17
2	343±9
1	344±5

Fig. 5. (a) DLS intensity-weighed size distributions obtained by CONTIN of PVDF-HFBII water dispersions at increasing PVDF concentrations as shown in the legend (HFBII concentration 0.1 mg/mL). (b) Averaged hydrodynamic sizes calculated from the size distribution graphs reported in (a), the reported uncertainty is the SD on three different measurements.

filming ability of 133 ng/cm^2, in reasonable agreement with the above mentioned literature values.

TEM analysis of PVDF-HFBII dispersions showed the presence of particles having an average size of 223 ± 31 nm, in agreement with the size obtained for the pristine PVDF dispersion in MEK (Fig. 3a and b). HFBII monolayer on hydrophobic surfaces has been shown to be about 2 nm thick [26]. Therefore, no significant impact on the NP size was expected upon HFB surface adsorption. Differently from TEM results, DLS analysis indicated a slight increase of the hydrodynamic radius of the particles, yielding a size of 297 ± 4 nm. This is likely due to the formation, driven by the protein monolayer surrounding the polymeric particles, of a hydration shell around the NP surface. In fact, it is well known that HFBII binds to hydrophobic surfaces via its hydrophobic patch, exposing the more hydrophilic amino acids to the more polar environment [25,27]. This ability of turning the nature of

a surface from hydrophobic to hydrophilic through the formation of an amphiphilic HFBII film has been exploited here for dispersing highly hydrophobic PVDF NPs in water. The presence of the HFBII film can clearly be seen in the TEM images reported in Fig. 4, which compares PVDF particles with and without HFBII coating. In Fig. 4b the HFBII coated PVDF NPs' surface appears much less smooth and regular than in pristine PVDF NPs (Fig. 4a).

Size distributions obtained by DLS analysis of PVDF-HFBII water dispersions at different PVDF concentrations are shown in Fig. 5. Values reported in the table of Fig. 5 show that the average hydrodynamic size of the NPs increases on increasing polymer concentrations. This size increase was also accompanied by a significant decrease in the polydispersity (narrower width of the size distributions) of the system that might be due to a lower concentration of free HFBII in the dispersion as the free protein

Fig. 6. ATR-FTIR spectra of the pristine PVDF nanostructured powder (light blue curve), solid HFBII (dark blue curve), and of the freeze-dried PVDF-HFBII powder obtained from the 1 mg/mL dispersion (red curve). (For interpretation of the references to color in this figure legend, the reader is referred to the web version of the article.)

may partly contribute to the scattering, increasing the polydispersity of the system.

The class II hydrophobin HFBI, which has similar self-assembly features to those of HFBII, was also successfully tested for dispersing PVDF NPs in water. PVDF-HFBI aqueous dispersions (PVDF concentration 1 mg/mL) yielded NPs having a size of 306 ± 15 nm, slightly smaller than those obtained with HFBII at the same PVDF and protein concentrations (see ESI Fig. S2).
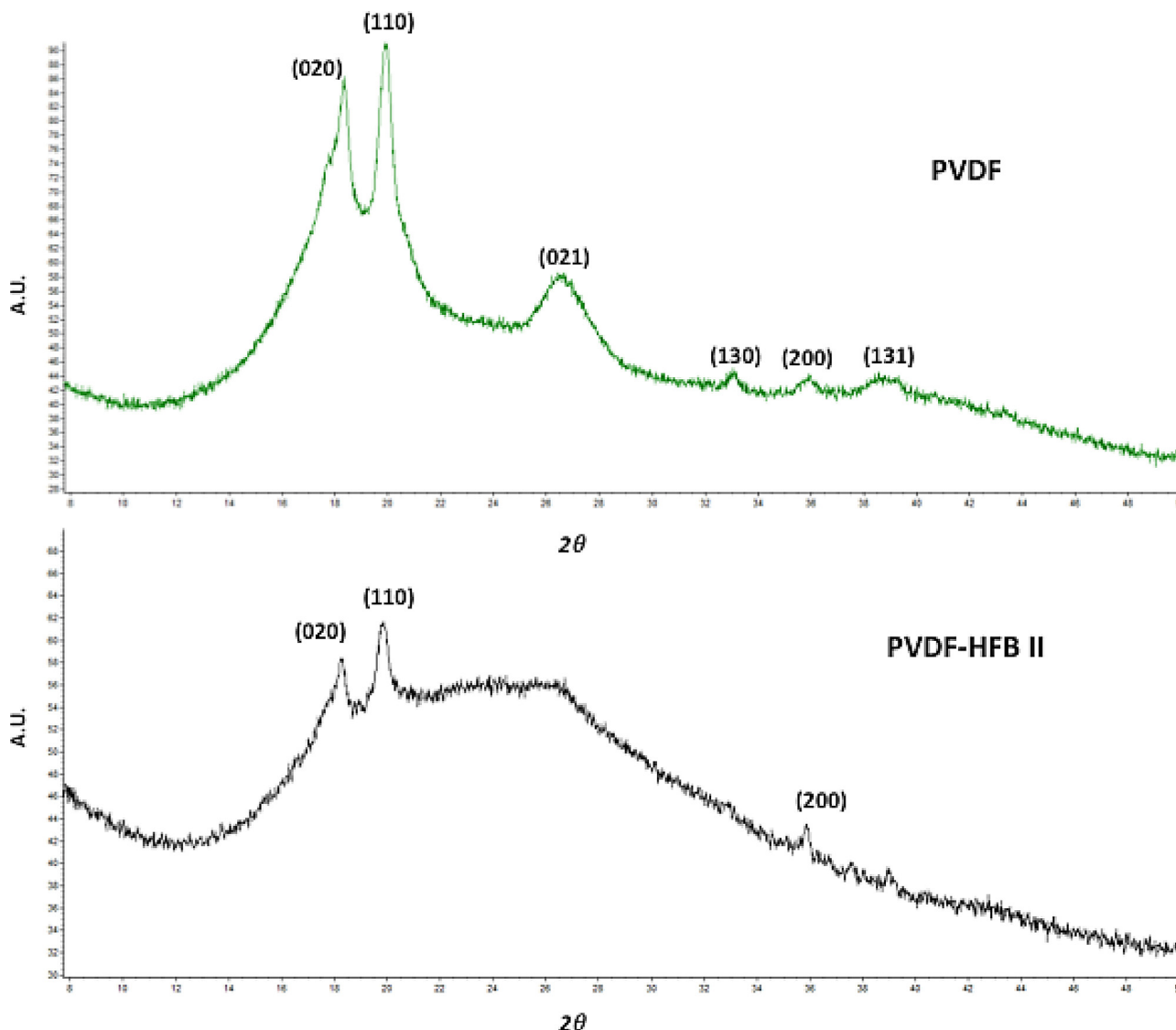
Both HFBI and HFBII were efficient in coating PVDF NPs, making them hydrophilic and dispersible in water. To date no environmentally friendly PVDF water dispersions have been reported in literature. Due to the easy preparation methodology reported here and the high reproducibility of the process, the use of HFB might open new perspectives in the applications of PVDF.

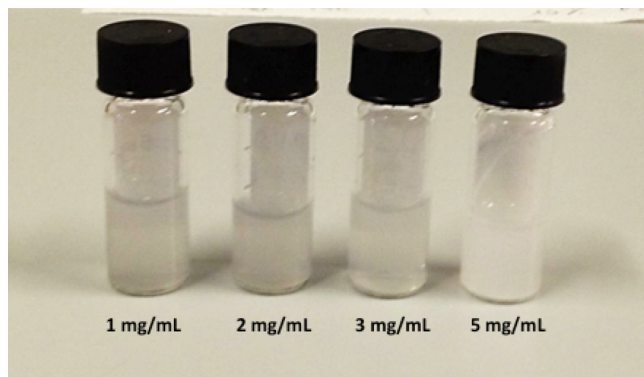## 2.2. Solid state characterization of PVDF-HFBII freeze-dried dispersions

Attenuated total reflectance-Fourier transform infrared spectroscopy (ATR-FTIR) and X-ray diffraction (XRD) techniques have been extensively used for the identification and characterization of PVDF structural features either as pure polymer or blended with other polymers or small molecules [5]. It is well known that PVDF has a highly polymorphic behaviour and can crystallize into five possible forms, namely α, β, γ, δ, and ε, depending on crystallization conditions [24]. The most common crystalline form is the nonpolar α-phase with the TGTG conformation. The β- and γ-phase, which have TTT planar zigzag and TTTGTTTG conformations, respectively, are polar and thus responsible for the piezo and ferroelectrical properties of the polymer. The two other crystal phases are rarely observed.

We considered of interest to assess the prevailing form in the PVDF NPs we coated with HFB, in order to study whether the chosen protocol may affect crystallinity. Information on the structural characteristics of our pristine PVDF was obtained from detailed analysis of the IR region between 450 and 1400 cm^{-1} (Fig. 6, top). The presence of the α form in our starting PVDF NPs was shown by the identification of the bands at 1150 cm^{-1} (CF$_2$ symmetric stretching mode) and at 976 cm^{-1} (CH$_2$ twisting mode), which are exclusively present in this polymer phase [24,29]. The detection of additional CF$_2$ bending modes (490.9, 613.9 and 762.7 cm^{-1}) and CH out-of-plane deformation bands (873.8 cm^{-1}) in the spectrum confirmed the identity of the α phase.

Fig. 7. Powder XRD patterns for the pristine PVDF nanostructured powder (above) and the freeze-dried PVDF-HFBII powder obtained from the 1 mg/mL PVDF dispersion (below). The crystallographic planes are labelled.

Fig. 8. PVDF–HFBII water dispersions obtained by re-dispersion of freeze-dried powders at different PVDF concentrations as labelled on the vials.

Further proof of the α phase of the starting PVDF was gained by powder XRD studies. The powder pattern (Fig. 7, top) shows peaks at *2θ* equal to 18.05, 19.95, 25.85, 33.05, 35.81, and 38.72°, corresponding to the diffractions in planes (020), (110), (021), (130), (200), and (131), respectively, all characteristic of the α-phase [30].

DSC analysis of the pristine PVDF showed a melting peak at 158.8 °C (see ESI, Table S1), as expected for the α-form. A comparison between the area of this peak and the enthalpy of fusion of a 100% α-phase crystalline PVDF reported in the literature (ΔH_{fusion}: 104.6 J/g) allowed for a rough estimation of the degree of crystallinity for our sample, which was found to be around 40%. ATR-FTIR analysis was successively performed also on solid HFBII and freeze-dried PVDF (1 mg/mL)-HFBII dispersions. The main peak visible in the HFBII spectrum is related to the strong amide I (1624 cm^{-1}) signal, corresponding to the C=O vibrations of the HFBII peptide bonds. Fig. 6 clearly shows a broadening of the amide I band together with a shift from 1624.7 cm^{-1} for the pure HFBII, to 1644.7 cm^{-1} for the freeze-dried PVDF-HFB dispersion. This shift may suggest a change in the protein secondary structure upon binding to the PVDF surface [31], and is in agreement with the increase of α-helix content described in the literature for protein assembling at water–hydrophobic interfaces [32].

The powder X-ray diffraction (PXRD) pattern of the freeze-dried PVDF-HFBII obtained from the 1 mg/mL PVDF sample presents several peaks distributed over a broad bump characteristic of an amorphous state (see Fig. 7). This pattern suggests a reduction of the overall PVDF crystallinity, likely due to the procedure adopted for dispersing the polymer in the HFBII aqueous solution. The decrease of crystallinity in the protein-treated sample was also confirmed by DSC measurements, which showed a decrease of the PVDF crystallinity, possibly to 30% from the 40% of the pristine PVDF.
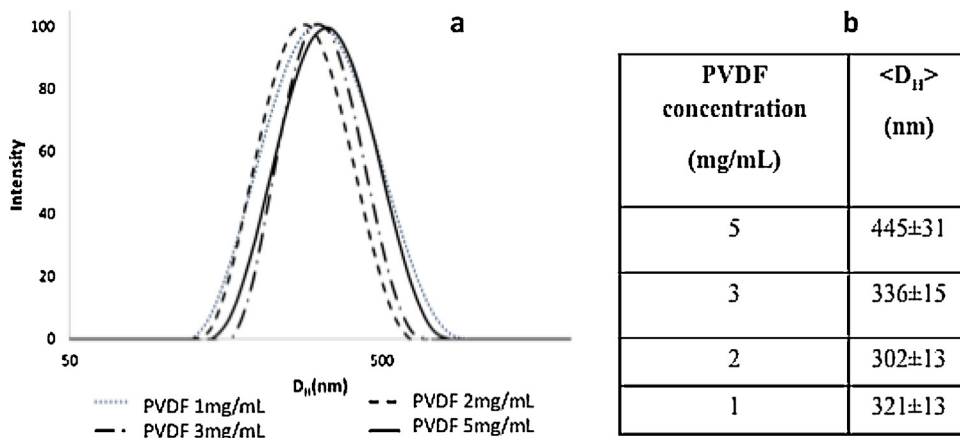
Moreover, the diffractogram, specifically the characteristic peaks at *2θ* equal to 18.3, 19.85, 35.87, and 39°, underlines how the prevailing crystalline phase of the polymer in the HFB-coated PVDF is the α-form as in the starting material. This result, in agreement with the FTIR data, suggests that the formation of the protein monolayer surrounding the PVDF particles does not influence the crystallinity of the polymer, which maintains largely unchanged its bulk structural properties. Similar PXRD patterns were also observed when incremental amounts of polymer were used in the formation of the bio-nanocomposites, i.e., 2 mg/mL, 3 mg/mL, and 5 mg/mL. In all of the samples, no change in the crystalline phase of the polymer compared to the 1 mg/mL was detected (see ESI).

2.3. Solid PVDF-HFBII bio-nanocomposite redispersion in aqueous environment

PVDF-HFBII dispersions were freeze-dried and stored in anhydrous environment for a week. Freeze-dried powders were subsequently re-dispersed in water and left for equilibration at room temperature for 24 h. As shown by Fig. 8, no polymer sedimentation was observed after 24 h. Therefore, the water dispersibility of PVDF particles mediated by HFBII was not affected by lyophilization. This indicates that the HFBII monolayer on PVDF NPs is likely to be kept intact during the lyophilization process as also suggested by the solid-state characterization of the lyophilized powders.

Re-dispersed PVDF-HFBII samples were analyzed by DLS and obtained results (Fig. 9) are in good agreement with size values obtained for the fresh samples, although a slight increase in size can be seen for all the PVDF starting concentrations.

The re-dispersibility of freeze-dried PVDF-HFBII powder renders the possible application of such systems even more convenient. Indeed, the possibility to store the dispersions in their dried state is expected to improve their stability avoiding potential particles aggregation in solution over time as well as possible solution contaminations.

PVDF concentration (mg/mL)	$\langle D_H \rangle$ (nm)
5	445±31
3	336±15
2	302±13
1	321±13

Fig. 9. DLS intensity-weighted size distributions obtained by CONTIN of PVDF-HFBII water re-dispersions at increasing PVDF concentrations as shown in the legend reported in the inset of the figure (HFBII concentration 0.1 mg/mL). The table on the left reports the average hydrodynamic diameters obtained by the size distributions reported in the figure.

3. Conclusions

This study proved the ability of class II hydrophobins, HFBI and HFBII, to reverse the surface wettability of PVDF NPs. In particular, HFBII was able to film PVDF surface with a maximum filming capacity of approximately 133 ng/cm^2, yielding monodispersed PVDF NPs aqueous dispersions as shown by DLS analysis. HFBII coating on PVDF NPs was also imaged by TEM analysis. HFBII-coated PVDF NPs resulted to be stable in aqueous solutions over time and easily re-dispersible after freeze-drying, showing the resistance of the HFB film to this process. Lyophilized PVDF-HFB bio-nanocomposites were studied by ATR-FTIR, XRD, and DSC, which indicated protein adsorption on the NP surface and minor changes of the crystallinity (α-form) of the polymer during the coating protocol. The possibility of dispersing PVDF NPs in aqueous solutions without significantly affecting their size or changing the polymer crystalline phase may open the use of PVDF to new applications. In fact, the obtained PVDF-HFBII bio-nanocomposites dispersions represent, to the best of our knowledge, the first environmentally friendly dispersions of PVDF NPs in water. The use of such aqueous PVDF dispersions will be tested in some of the current applications of this polymer, which otherwise requires the use of organic solvents or high temperature process, bringing forth a more sustainable approach. In particular, the newly developed PVDF water dispersions might be employed, upon HFB calcination, as surface coating materials. Furthermore, freeze-dried PVDF-HFBII bio-nanocomposites might potentially find application as polymer nanofillers for hydrophilic matrices, a field of research that is currently under investigation in our laboratories.

4. Materials and methods

4.1. Chemicals

HFBII was obtained as described in [33]. PVDF was obtained from Solvay Specialty Polymers (Hylar® 301 F). Reagents were used without further purification. Milli-Q water (mQW) was obtained by a Simplicity (Millipore) instrument.

4.2. Preparation of the samples

Accurately weighed PVDF was dispersed in mQ water and vortexed at 30 rpm for 1 min. Three cycles of 1 min ultrasonication were performed using a SONIC Vibracell operating at 20 V. Before measuring, samples were left at room temperature for 24 h to allow equilibration.

4.3. TEM analysis

TEM images were acquired by using a Philips CM200 TEM, equipped with a field emission gun and operating at 200 kV. PVDF and PVDF-HFBII dispersions were prepared by dropping the sample solution on carbon-coated copper grids. Due to the intrinsic low contrast of organic materials, negative staining of PVDF-HFBII samples was performed by using uranyl acetate (1%, w/v). Both samples were left drying overnight. TEM statistical analysis was based on the measurement of about 100–150 NPs. Size distributions were fitted by a Gaussian equation using Igor Pro 4.02.

4.4. DLS

DLS experiments were carried out using a Zetasizer Nano ZS (Malvern Instrument, Malvern, Worcestershire, UK), equipped with a 633 nm red laser and measuring the scattered light at an angle of 173°. Samples were analyzed 24 h after preparation. Measurements were performed at 25 °C and each measurement consisted of 5 runs and was averaged on 3 replicates.

4.5. Solid state analysis

PVDF-HFBII dispersions were freeze-dried using a Edwars Modulyo EF4-1596 (Edwards, Crawley, West Sussex, UK).

Attenuated total reflectance-Fourier transform infrared (ATR-FTIR) analysis was performed on freeze-dried samples using a Thermo Scientific Nicolet iS50 FT-IR spectrometer, equipped with a iS50 ATR accessory (Thermo Scientific, Madison, USA). 32 scans were collected for each sample at a resolution value of 2 cm^{-1}.

A Bruker AXS D8 powder diffractometer was used for all powder X-ray (PXRD) measurements. Experimental parameters are as follows: Cu-Ka radiation (λ = 1.54056 Å), scanning interval: 6–60° 2θ. Step size: 0.016°. Exposure time 1.5 s/step.

Appendix A. Supplementary data

Supplementary data associated with this article can be found, in the online version, at http://dx.doi.org/10.1016/j.jfluchem.2015.02.004.

References

[1] H. Kawai, Jpn. J. Appl. Phys. 8 (1969) 975–976.
[2] K. Nakamura, Y. Wada, J. Polym. Sci. A: Polym. Phys. 9 (1971) 161–173.
[3] E. Fukada, T. Furukawa, Ultrasonics 19 (1981) 31–39.
[4] S.B. Lang, Trans. Electr. Insul. 24 (1989) 503–516.
[5] B. Ameduri, Chem. Rev. 109 (2009) 6632–6686.
[6] G. Kang, Y. Cao, J. Membr. Sci. 463 (2014) 145–165.
[7] N. Durand, P. Gaveau, G. Silly, B. Ameduri, B. Boutevin, Macromolecules 27 (2011) 6249–6257.
[8] N. Durand, B. Boutevin, G. Silly, B. Ameduri, Macromolecules 27 (2011) 8487–8493.
[9] N. Durand, D. Mariot, B. Ameduri, B. Boutevin, F. Ganachaud, Langmuir 27 (2011) 4057–4067.
[10] H. Sawada, T. Tashima, Y. Nishiyama, M. Kikuchi, Y. Goto, G. Kostov, B. Ameduri, Macromolecules 44 (2011) 1114–1124.
[11] M.J. Kershaw, N.J. Talbot, Fungal Genet. Biol. 23 (1998) 18–33.
[12] Please see the web-site: http://www.kynaraquatec.com/en/index.html.
[13] M.B. Linder, Curr. Opin. Colloid Interface Sci. 14 (2009) 356–363.
[14] J.M. Kallio, M.B. Linder, J. Rouvinen, J. Biol. Chem. 282 (2007) 28733–28739.
[15] S.O. Lumsdon, J. Green, B. Stieglitz, Colloids Surf. B 44 (2005) 172–178.
[16] M.B. Linder, G.R. Szilvay, T. Nakari-Setala, M.E. Penttila, FEMS Microbiol. Rev. 29 (2005) 877–896.
[17] G. Israeli-Lev, Y.D. Livney, Food Hydrocolloid 35 (2014) 28–35.
[18] G. Fang, B. Tang, Z. Liu, J. Gou, Y. Zhang, H. Xu, X. Tang, Eur. Pharm. Sci. 60 (2014) 1–9.
[19] M. Sarparanta, L.M. Bimbo, J. Rytkönen, E. Mäkilä, T.J. Laaksonen, P. Laaksonen, M. Nyman, J. Salonen, M.B. Linder, J. Hirvonen, H.A. Santos, A.J. Airaksinen, Mol. Pharm. 9 (2012) 654–663.
[20] M.P. Monopoli, C. Åberg, A. Salvati, K.A. Dawson, Nat. Nanotechnol. 7 (2012) 779–786.
[21] R. Milani, E. Monogioudi, M. Baldrighi, G. Cavallo, V. Arima, L. Marra, A. Zizzari, R. Rinaldi, M.B. Linder, G. Resnati, P. Metrangolo, Soft Matter 9 (2013) 6505–6514.
[22] A.H.Y. Kwan, R.D. Winefield, M. Sunde, J.M. Matthews, R.G. Haverkamp, M.D. Templeton, J.P. Mackay, Proc. Natl. Acad. Sci. U. S. A. 103 (2006) 3621–3626.
[23] H. Wosten, O. De Vries, J. Wessels, Plant Cell 5 (1993) 1567–1574.
[24] Y.J. Park, Y.S. Kang, C. Park, Eur. Polym. J. 41 (2005) 1002–1012.
[25] M.S. Grunér, G.R. Szilvay, M. Berglin, M. Lienemann, P. Laaksonen, M.B. Linder, Langmuir 28 (2012) 4293–4300.
[26] X.L. Zhang, J. Penfold, R.K. Thomas, I.M. Tucker, J.T. Petkov, J. Bent, A. Cox, Langmuir 27 (2011) 10464–10474.

[27] Z. Wang, M. Lienemann, M. Qiau, M.B. Linder, Langmuir 26 (2010) 8491–8496.

[28] K. Kisko, G.R. Szilvay, E. Vuorimaa, H. Lemmetyinen, M. Torkkeli, R. Serimaa, Langmuir 25 (2009) 1612–1619.

[29] Y. Bormashenko, R. Pogreb, O. Stanevsky, E. Bormashenko, Polym. Test. 23 (2004) 791–796.

[30] R. Hasegawa, Y. Takahashi, Y. Chatani, H. Tadokoro, Polym. J. 3 (1972) 600–610.

[31] M.L. De Vocht, I. Reviakine, W.-P. Ulrich, W. Bergsma-Schutter, H.A.B. Wösten, H. Vogel, A. Brisson, J.G.H. Wessel, G.T. Robillard, Protein Sci. 11 (2002) 1199–1205.

[32] S. Askolin, M.B. Linder, K. Scholtmeijer, M. Tenkanen, M. Penttilä, M.L. de Vocht, H.A.B. Wösten, Biomacromolecules 7 (2006) 1295–1301.

[33] M.B. Linder, K. Selber, T. Nakari-Setälä, M. Qiao, M.R. Kula, M. Penttilä, Biomacromolecules 2 (2001) 511–517.